

## Fluctuations at the critical state of a polygonal packing

A.A. Peña<sup>1,\*,\dagger</sup>, A. Lizcano<sup>2</sup>, F. Alonso-Marroquin<sup>3</sup> and H. J. Herrmann<sup>4</sup>

<sup>1</sup> *Institute for Computational Physics, Pfaffenwaldring 27, 70569 Stuttgart, Germany*

<sup>2</sup> *Universidad de los Andes, Bogotá D.C., Colombia*

<sup>3</sup> *Earth Systems Science Computational Centre, The university of Queensland, Sta. Lucia, Australia*

<sup>4</sup> *Institut für Baustoffe, ETH-Höenggerberg, Zürich, Switzerland*

### SUMMARY

The mechanical response of cohesionless granular materials under monotonic load is studied by performing molecular dynamic simulations. The diversity of shapes of soil grains is modeled by using randomly generated convex polygons as granular particles. Results of the biaxial test obtained for dense and loose media show that samples achieve the same void ratio at large strains independently of their initial density state. This limit state resembles the so-called critical state of soil mechanics, except for some stress fluctuations, which remain for large deformations. These fluctuations are studied at the micro-mechanical level, by following the evolution of the coordination number, force chains and the fraction of the sliding contacts of the sample. Copyright © 2006 John Wiley & Sons, Ltd.

KEY WORDS: Granular material; biaxial test; critical state; interparticle friction; force fluctuations

### 1. INTRODUCTION

The stress-strain response of granular materials shows a nonlinear and irreversible behavior when they are subjected to external load. This macro-mechanical behavior stems from the discrete character of the media and phenomena occurring at the grain scale.

Numerical simulations using the discrete element method (DEM) have become a valuable tool in the study of different phenomena occurring at the micro-mechanic scale in granular materials [1] and [2]. DEM is a powerful way to explore the behavior of granular media on both the micro- and macro levels, as a complement to standard experimental data. The mechanical response of the media is obtained by modeling the particle interactions as a dynamic process and using simple mechanical laws in these interactions. Generally, discrete models use discs or spheres to reduce the time of calculation; however, these kind of models do not consider the effect of particle shape on the mechanical behavior. Several researchers have studied this influence; for example, Holubec and D'Appolonia [1] concluded that the variation order of the mechanical properties due to the shape of the particle, could be of the same magnitude as the

---

\*Correspondence to: Institute for Computational Physics, Pfaffenwaldring 27, 70569 Stuttgart, Germany

<sup>\dagger</sup>E-mail: andres@ica1.uni-stuttgart.de

variation due to the changes in density. By means of numerical simulations, Mirghasemi et al. [3] demonstrated that the particle angularity has an important effect in the compressibility and shear strength of the granular media. Alonso-Marroquin et al [4] show also that angularity significantly affect the force distribution inside the granular media, and hence the elasto-plastic response of the materials. It is therefore very important to take into account the particle shape in order to have a more realistic soil representation.

Force fluctuations under quasi-static load is another aspect that is affected by particle shape. They appear as a consequence of frictional instabilities. Fluctuations are observed in glass bead samples [5] and packings of glass spheres [6]. Experimental biaxial tests show evidence of *dynamic instabilities* at the critical state [7]. Erratic slip-stick motion at the critical state is interesting, owing to its potential analogy with earthquake dynamics [8]. In this paper we investigate stress fluctuations by means of molecular dynamics simulations of biaxial test. In order to include the effect of the diversity of shapes of a realistic soil, The grains are represented by randomly generated convex polygons. We show that the granular media evolve toward the critical state, where fluctuations of stress and abrupt collapse of the number of sliding contacts characterize the dynamic response.

The outline of this paper is as follows. The discrete model and the sample specifications are introduced in Section 2. In Section 3 we show that the biaxial test simulations reproduces the main features of the critical state in soil mechanics. The stress fluctuations and its correlation to the micro-mechanical variables is presented in Section 4. Finally, in Section 5 conclusions are exposed.

## 2. MODEL

The random generation of the convex polygons used in this model is carried out by means of a Voronoi tessellation. This is a simple method to discretize the media without introducing any kind of anisotropy [9]. The distribution of areas of polygons is symmetric around its mean value  $1 \text{ cm}^2$ , and follows approximately a Gaussian distribution with variance of  $0.36 \text{ cm}^2$  (Figure 1). The number of edges of the polygons is distributed between 4 and 8 for 98.7% of polygons (Figure 2).

Once the sample has been created each particle is subjected to interparticle forces and boundary forces. It is assumed that particles interact elastically with each other. The polygons can neither be broken nor deformed, but they can overlap when they are pressed against each other. This overlap represents the local deformation of the grains. This approach has been thoroughly used to model many different processes, such as strain localization and earthquakes [2], fragmentation [10], and damage [11]. When all forces  $F_i$  acting on the particle  $i$ ,  $F^c$  from interparticle contacts and  $F^b$  from boundaries are known, the evolution of the position  $\vec{x}_i$  and orientation  $\theta_i$  of the  $i$  polygon is given by the integration of Newtons's equation of motion:

$$-m_i \ddot{\vec{x}}_i + \sum_c \vec{F}_i^c + \sum_{c_b} \vec{F}_i^b = \vec{0} \quad (1)$$

$$-I_i \ddot{\theta}_i + \sum_c \vec{l}_i^c \times \vec{F}_i^c + \sum_{c_b} \vec{l}_i^b \times \vec{F}_i^b = \vec{0} \quad (2)$$

where  $m_i$  denotes the mass of particle  $i$ ,  $I_i$  its moment of inertia and  $\vec{l}$  the branch vector which

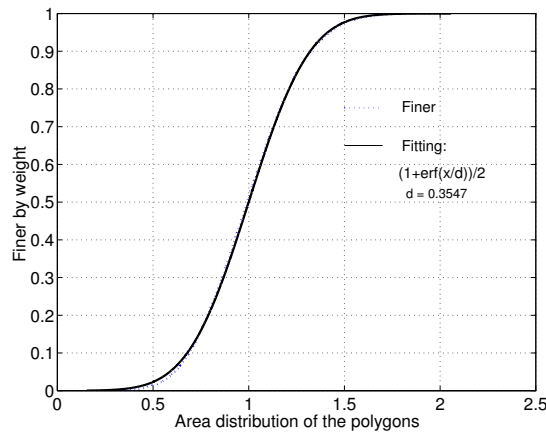


Figure 1. Cumulative distribution of polygon areas. The solid line shows the fit of the data using an error function. The distribution is calculated for  $1.8 \times 10^4$  polygons.

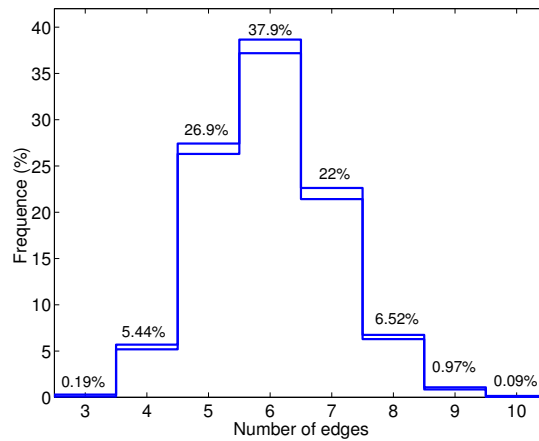


Figure 2. Distribution of number of edges. Five different generations, each one with 3600 polygons, were used in the calculations. The bars show the standard deviation of the data.

connects the center of mass of the polygon to the application point of the contact force. Each particle has two linear and one rotational degrees of freedom. In the following section the laws of the contact forces are introduced.

2.1. Contact law

The contact force results from the overlap area  $a$  between particles. In Figure 3 the configuration of a particle contact is presented,  $P_1$  and  $P_2$  represent the intersection points between the edges of the polygons; the segment that connects those points gives the contact line  $\vec{S} = P_1P_2$ . This vector defines a coordinate system at the contact  $(\hat{n}, \hat{t})$ ; where  $\hat{n}$  and  $\hat{t} = \vec{S}/|\vec{S}|$  normal to it give the direction of the normal  $F_n$  and tangential  $F_t$  components of the contact force. The point of application of the contact forces is taken as the center of mass

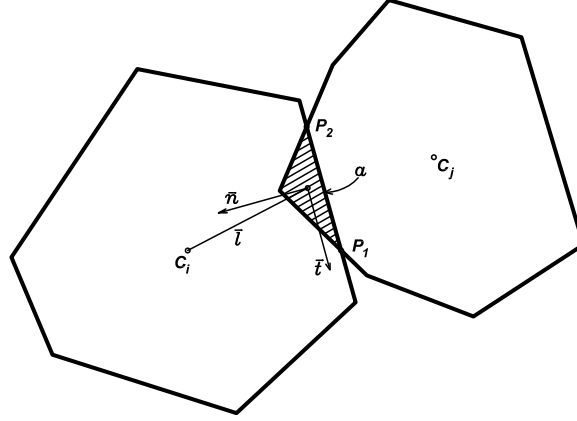


Figure 3. Schematic representation of a particle contact, the overlapping area  $a$  is indicated by the shaded zone.

of the overlap area [12].

The contact force is calculated as:

$$\vec{F}^c = -k_n \delta \hat{n} - k_t \xi \hat{t} \quad (3)$$

where  $k_n$  and  $k_t$  are the stiffnesses at the contact in the respective directions. The deformation length  $\delta$  is equal to  $a/|\vec{S}|$ . The tangential force is introduced by an elastic spring whose displacement  $\xi$  is equal to 0 for new contacts, while for old contacts the tangential spring-length is obtained as follows,

$$\xi = \xi' + \vec{v}_i^c \Delta t_{MD}, \quad (4)$$

where  $\xi'$  is the previous length of the spring,  $\Delta t_{MD}$  is the time step of the molecular dynamic simulation, and  $\vec{v}_i^c$  the tangential component of the relative velocity  $\vec{v}^c$  at the contact:

$$\vec{v}^c = \vec{v}_i - \vec{v}_j + \vec{\omega}_i \times \vec{l}_i - \vec{\omega}_j \times \vec{l}_j. \quad (5)$$

here  $\vec{v}_i$  is the linear velocity and  $\vec{\omega}_i$  is the angular velocity of the particles in contact. The elastic tangential displacement  $\xi$  at the contact increases until the Coulomb's sliding condition  $|F_t^c| = \mu F_n^c$  is reached. Here the sliding condition is enforced keeping constant the tangential force. Finally, we introduce a viscous force (Eq. 6), which is necessary to maintain the numerical stability of the method and to obtain a quick convergence to the equilibrium configuration.

$$\vec{F}_v^c = -m(\nu_n \cdot \vec{v}_n^c \cdot \hat{n}^c + \nu_t \cdot \vec{v}_t^c \cdot \hat{t}^c) \quad (6)$$

where  $m = (1/m_i + 1/m_j)^{-1}$  is the effective mass of the two particles in contact, and  $\nu_n$  and  $\nu_t$  are the damping coefficients. This damping force leads to velocity-independent normal and tangential restitution coefficients. These coefficients of restitution are given by the ratio

between the relative velocity after and before the collision. In particular, the normal restitution coefficient  $\epsilon_n$  and  $\nu_n$  are related by the following expression [2]:

$$\epsilon_n = \exp\left(\frac{-\pi\nu_n}{\sqrt{\omega_n^2 - \nu_n^2}}\right) \quad (7)$$

where  $\omega_n = \sqrt{k_n/m_0}$ , and here  $m_0$  is the mean mass of the polygons. Using the parameters of Table I, we obtain a value of  $\epsilon_n$  equal to 0.73. This relatively low dissipation allows us to reduce viscous effects during loading.

## 2.2. Boundary conditions

During the simulation, the granular sample is confined by four rigid walls. These walls always maintain their horizontal or vertical orientation. Boundary forces are applied on each grain in contact with these walls. The walls are frictionless, so they transmit only normal forces to the polygons in contact with them. When one of the vertices of a polygon penetrates one of the walls, a force, proportional to the penetration length  $\delta$ , is applied on the polygon. This boundary force  $\vec{F}_n^b$  is oriented in normal direction  $\hat{n}$  to the wall (8).

$$\vec{F}_n^b = -k_n\delta\hat{n} \quad (8)$$

$$\vec{F}_v^b = -m_i\nu_n\vec{v}_n^c \quad (9)$$

Viscous forces  $\vec{F}_v^b$  in wall-polygons interactions are also considered (Eq. 9), where  $m_i$  is the mass of the particle in contact with the boundary wall, and  $\nu_n$  the damping coefficient in normal direction. The boundary force is calculated for all the cases of interaction between walls and polygons in the same way. Finally, the displacement of the walls and the total force on them are used to determine the global stress and strain of the assembly.

Table I. Parameters used in the model

Parameter	Ratio	Value
Friction coefficient	$\mu$	0.55
Normal stiffness	$k_n$	$1.6 \cdot 10^8$ N/m
Normal damping coefficient	$\nu_n$	$4000$ s <sup>-1</sup>
Stiffness ratio	$\zeta = k_t/k_n$	0.33
Viscosity ratio	$\nu_t/\nu_n$	0.33
Time ratio	$t_0/t_s$	1000
Time step	$\Delta t_{MD}$	$2.5 \cdot 10^{-6}$ s

## 2.3. Parameters of the model

The parameters used in the model are presented in Table I. The interparticle friction coefficient was chosen  $\mu = 0.55$ , which yields similar values of macro-mechanic friction angles to those obtained in real materials as gravel or sands [13]. The stiffness ratio  $\zeta = k_t/k_n$  as well as the viscosity ratio ( $\nu_t/\nu_n$ ) were taken 0.33. The normal stiffness  $k_n$  was taken  $1.6 \cdot 10^8$  N/m; and

the normal damping coefficient  $\nu_n = 4000 \text{ s}^{-1}$ . The viscosity factors were selected to preserve numerical stability and to reduce the acoustic waves produced during loading. Finally, the time ratio in Table 1 is the ratio between the time of loading  $t_0$  and the characteristic period of oscillation  $t_s = \sqrt{m_0/k_n}$ . The value of  $t_s$  determines the selection of the time step  $\Delta t_{MD}$ . We use a 5<sup>th</sup> order predictor-corrector integration scheme, which preserve stability whenever  $\Delta t < 0.10 \cdot t_s$  [14].

#### 2.4. Sample construction

After generation of the polygons, the sample is confined by applying a centripetal gravitational field to the particles and on the walls, oriented to the center of mass of the assembly. Then the sample is compressed isotropically until the desired confining pressure is reached. In order to generate dense samples, the interparticle friction is set to zero during the construction. The loose samples are created taking damping coefficients 100 times greater than those used in the test stage. In both cases, the parameters are set to the values shown in Table 1 after the preparation of the sample. The sample specifications used to perform the simulations were:  $1000 \text{ kg/m}^2$  for the density of particles, system size of 400 polygons, and a unitary shape ratio (width/height).

### 3. BIAXIAL TEST SIMULATIONS

In this test, the pressure in lateral walls  $\sigma_2$  is kept constant and the horizontal walls (axial direction) are moved with constant shear rate inducing deviatoric stress. The stress-strain behavior at the macro-mechanical scale, for dense and loose systems, and its dependence on some mechanisms at the micro-mechanical scale are discussed. The effect of the interparticle coefficient of friction on the macro-mechanical response of the media is also studied.

In the test the axial and lateral directions are indicated as 1 and 2, respectively. That is  $\sigma_1$  and  $\varepsilon_1$  are the axial stress and strain, and  $\sigma_2$  and  $\varepsilon_2$  are the lateral components. Stresses have the same sign convention used in soil mechanics: compressive normal stresses are positive and tensile normal stresses are negative.

The parameters used to perform the biaxial tests are presented in Table II.

Parameters	Value
Default confining pressure	160 kN/m
Axial strain rate	$0.02 \text{ s}^{-1}$
Maximum axial strain	20 %

#### 3.1. Macromechanical observations

Three different samples were used to evaluate the mechanical response of polygonal packings, each one corresponds to a different seed used in the random generation. The initial void ratios of the dense and loose samples are presented in Table III.

Figure 4(a) shows the evolution of  $\sin \phi = (\sigma_1 - \sigma_2)/(\sigma_1 + \sigma_2)$  with axial strain  $\varepsilon_1$  for the dense and loose system. In general, the dense samples exhibit a higher initial stiffness than

Table III. Initial void ratio of the samples

Sample	Dense state	Loose state
1	0.128	0.251
2	0.130	0.262
3	0.135	0.271

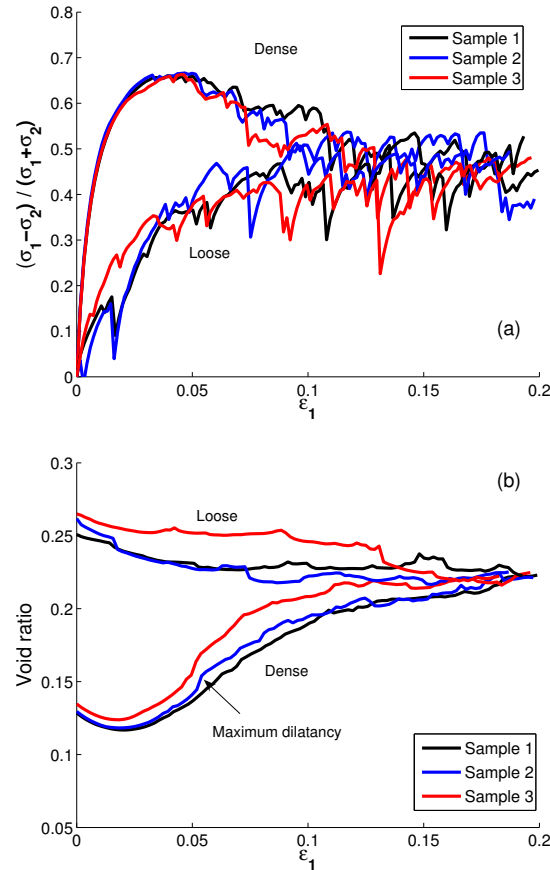


Figure 4. Evolution of (a) the deviator stress and (b) void ratio of the samples.

the loose ones. After the peak in the dense media, which is about 5% axial strain, a strain-softening behavior is observed. The loose media exhibit more frequent and bigger variations in the stress behavior. Additionally, a peak strength is not observed. Although an increase of fluctuations of the stress are observed for both systems at large deformations, it presents a tendency to stabilize around a value that one could consider as the steady state of the material ( $d\sin\phi/dt = 0$ ). The evolution of the void ratio with axial strain is illustrated in Figure 4(b). Initially, the dense samples contract and later the void ratio increases (dilatancy). For large

axial strain values the void ratio reaches a constant value. Comparing the evolution of dense samples in Figure 4(a) and (b) we notice that the maximum rate of dilatancy agrees with the peak strength (5% axial strain) which is expected on soils. It is especially observed in samples 2 and 3. The loose samples reduce their void ratio during the test (Fig. 4(b)), and it tends to a constant ratio near to 18% axial strain. The void ratio in both dense and loose samples varies until it achieves the same value near to 0.23 corresponding to 18% axial strain. In this stage, the granular medium is deformed at constant volume and with the same approximate value of deviator stress, which corresponds to the critical state of the material and it is independent of the initial sample density [15]. All these features reproduce the asymptotic behavior of soils obtained in laboratory experiments [16].

*3.1.1. Shear bands* Strain localization has been experimentally studied by several researchers in the last two decades, e.g. Vardoulakis [17], Desrues [18] and others. Using the discrete element method Cundall [19], and Bardet and Proubet [20] have studied this phenomenon. Theoretically, some authors have also investigated strain localization, for instance Vardoulakis [21], or Chambon et al. [22] by using the so-called second gradient method. In this paper a brief analysis of strain localization is performed by studying the displacement of the individual particles. In Figures 5 the displacement vectors of the particles for the dense assembly are presented. At the beginning of the test, the displacements are very small and one can observe approximately a symmetrical deformation around the center of the sample (Fig. 5(a)). As the axial strain increases and before the peak strength is reached a slight tendency to strain localization is observed. After having overcome the peak strength, the particle displacements seem to define independent bodies with different displacement directions (a clearer strain localization). This localization persists as the loading increases, and becomes clearer around 8.9 % axial strain (Fig. 5(b)), where two "shear bands" are observed. After peak, these shear bands are not constant in time. In fact, there are stages in which clear shear bands are observed, but they typically disappear when a drop on the stress occurs. These drops, as we will see in Section 4, are related to force chains collapse and therefore to restructurations of the media that hinder the persistence of the shear bands. The particle displacements of Figures 5(a) and (b) are taken from two consecutive time intervals, which correspond to an increment of 0.1 % of axial strain. Figure 5(c) presents the displacement at 20 % axial strain measured from the particle initial position. Here three bodies with different direction of displacement, and the areas (shear bands) defined between them are visible.

Although the particle displacements of loose samples are not shown, their evolution reflects the force chains collapse and consequent rearrangement of the particles within the sample. This is observed on the large displacements of the particles which are associated to the drops of the stress-strain behavior [23]. Strain localization is not clear in loose media.

Concerning shear band orientation, most of the experimental data from biaxial tests on sand report that this orientation lies between the Mohr-Coulomb solution  $\theta_C = 45^\circ + \varphi/2$  and the Roscoe Solution  $\theta_R = 45^\circ + \Psi/2$  [24]. The latter is defined by the angle of dilatancy  $\Phi = \arcsin(d\varepsilon_V/d\gamma)$ , being  $d\varepsilon_V$  and  $d\varepsilon_\gamma$  the increments of volumetric and deviatoric strains at failure [25]. We observe that the inclination angle of the shear bands in Figure 5(c) are approximately between  $52^\circ$  and  $58^\circ$ . In this case, for  $\phi_{micro} = 28.8^\circ$  (Fig. 7)  $\varphi \approx 26^\circ$  and  $\Phi \approx 15^\circ$  the predictions of Mohr-Coulomb and Roscoe Solution define with very good agreement the limits for the angles found in the simulation.

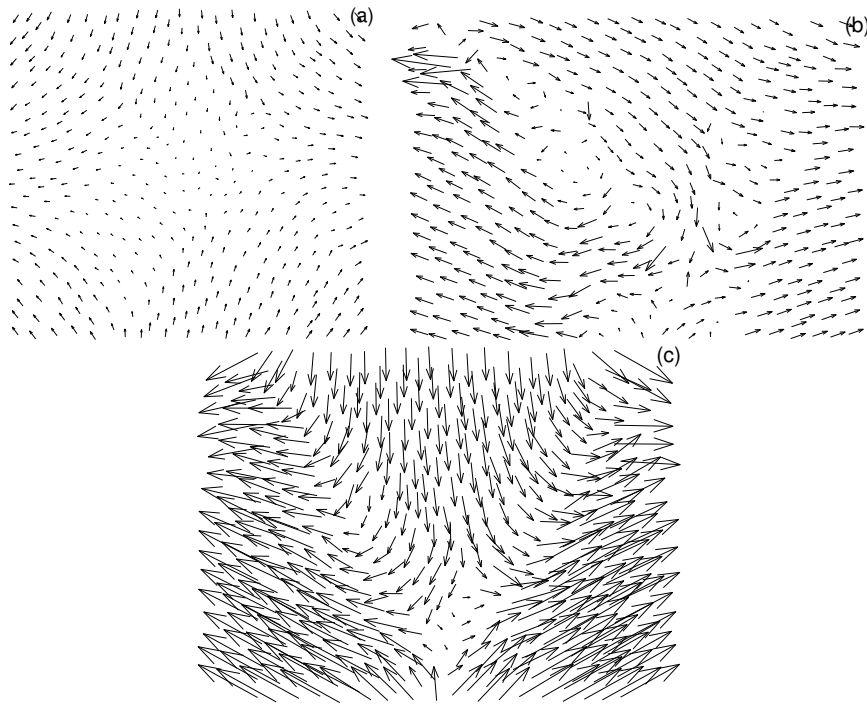


Figure 5. Displacement of particle centers within a dense sample at three axial strains (a) 1.2 %, (b) 8.9% and (c) 20% of total.

*3.1.2. Macroscopic friction* An approach to connect the Coulomb friction at the grain level to the macro-mechanical friction is to construct the Mohr-Coulomb failure surface of the granular sample. This failure surface can be obtained from the envelope of the Mohr circles at the peak stress value from biaxial tests [24]. The tests were carried out on dense samples, at three confining pressures: 80, 160 and 320 kN/m. Different methods are used to describe the failure surface of granular soils. In the following analysis, as used in traditional soil mechanics, we assumed that the failure surface is linear. Figure 6 shows the failure envelope of a granular sample with interparticle friction coefficient  $\mu = 0.55$  that corresponds to an interparticle friction angle  $\phi_{micro}$  of  $28.8^\circ$  ( $\mu = \tan \phi$ ). The envelope is traced as a tangent straight line to the Mohr circles, and the angle of friction of the bulk material is approximately  $41^\circ$ .

If we compare this result with the one obtained by Bardet using DEM with disks [26], we can then observe the important influence of particle shape on the macro-mechanical angle  $\phi_{peak}$  of the medium. For instance, using very similar values of  $\phi_{micro}$ ,  $28.8^\circ$  for polygons and  $26.5^\circ$  for disks, the obtained values of  $\phi_{peak}$  are  $41^\circ$  and  $22^\circ$  respectively. The ratio  $\phi_{peak}/\phi_{micro}$  is then equal to 1.42 for polygons and 0.83 for disks. Furthermore, as mentioned in the previous Section, different macro-mechanical angles are correlated to different orientation of strain localization (shear band). In the case of disks, if particle rotation is constrained, as in Ref. [26], a value of  $\phi_{peak} = 41^\circ$  is obtained. In such case, although  $\phi_{peak}$  is equal to the value for polygons, the sample dilatancy is almost completely hindered and therefore the stress-strain behavior of the sample is highly affected. For example, no correlation between peak strength

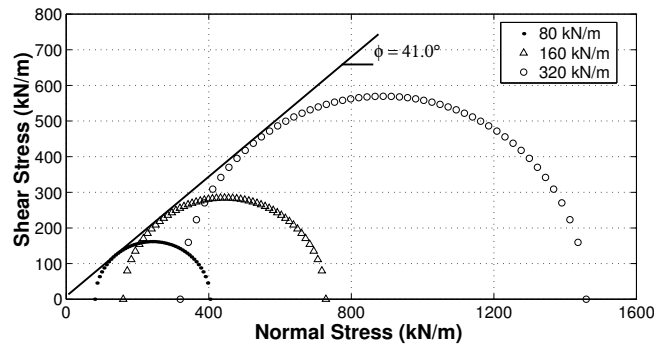


Figure 6. Mohr-Coulomb failure envelope constructed from biaxial test and Mohr circles. Interparticle friction angle  $\phi_{micro} = 28.8^\circ$ .

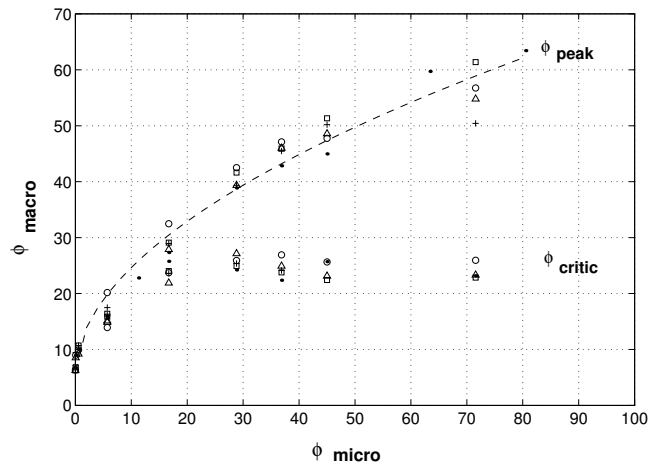


Figure 7. Evolution of the macro-mechanical friction angle. The dashed line is a power law approximation  $\phi_{peak} = 5.5 \cdot \phi_{micro}^{0.53} + 6$ .

and maximum rate of dilatancy is observed. All these observations confirm the important role of particle shape on the global behavior of granular media.

In order to study the effect of the interparticle friction  $\phi_{micro}$  on the macro-mechanical friction angle  $\phi_{macro}$ , different interparticle friction coefficients and five different samples were used in the simulations. Additional to the friction angle at the peak stress  $\phi_{peak}$ , the friction angle at the critical state  $\phi_{critic}$  was also calculated. Figure 7 shows for the five samples the values of  $\phi_{peak}$  and  $\phi_{critic}$  obtained from variations of  $\phi_{micro}$ . It is observed that at very low values of  $\phi_{micro}$  the macro-mechanical angles are quite similar. For values of interparticle friction angle larger than  $15^\circ$  the granular samples develop a clear peak strength  $\phi_{peak}$  (value different from  $\phi_{critic}$ ), while the  $\phi_{critic}$  value remains approximately constant. The last agrees with the experimental results obtained by Skinner [27], excluding the results from micro-mechanical angle close to zero. These results suggest that, except at small values of  $\phi_{micro}$  where friction does not play an important role, the friction angle mobilized at the critical

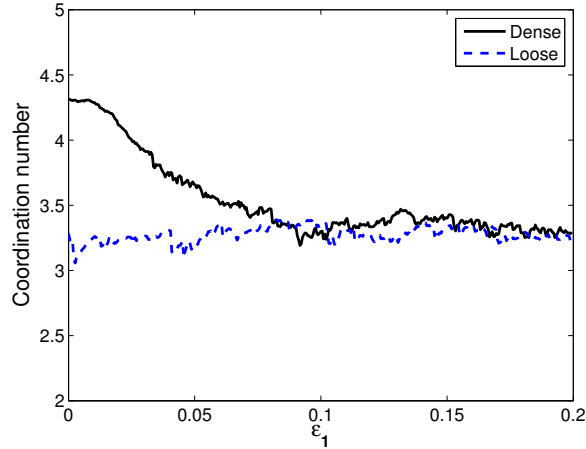


Figure 8. Evolution of the average coordination number during the biaxial test.

state  $\phi_{critic}$  is independent of the interparticle friction coefficient. This particular feature has been also observed in numerical simulations with circular particles [8]. The non-dependence of macroscopic friction on contact friction is attributed to the spontaneous formation of rotational patterns, such as the vorticity field shown in the Part (b) of Figure 5, and clusters of particles with intense rolling. Those deformation modes have shown to reduce considerably the bulk friction with respect to the expected value of the simple shear deformation [8].

Note that setting  $\phi_{micro}$  to zero, a value of  $\phi_{macro}$  close to 6.0 is obtained. Although this value of  $\phi_{macro}$  is calculated from the average of the deviator stress, the frictionless granular media offers a small resistance to shear. This result contrasts with the absence of shear resistance, as was found by Thornton [28] on a system of frictionless spheres. The presence of shear strength in non-frictional granular media is rather questioned. Some authors claim that this is given by interlocking among particle caused by the angularity of their shape [7]. In our simulations, viscosity and inertia effects could produce a residual strength during loading. So that we can not judge the origin of such residual strength.

#### 4. STRESS FLUCTUATIONS

According to the Critical State Soil Mechanics, large shear deformations drive the granular specimen to limiting state. This state is characterized by an isochoric deformation, where the stress ratio and the frictional dissipation stay constant [16]. This is not exactly that our simulations show. Indeed, we find that samples with different densities reach the same critical state, where the density and the stress ratio stay approximately constant, except for some fluctuations. In this Section we investigate the onset of such instabilities exploring the time evolution of the microstructural variables. The simplest way to explore microstructural arrangement of the granular sample is by following the evolutions of the following two internal variables: (1) The coordination number and, (2) the fraction of sliding contact.

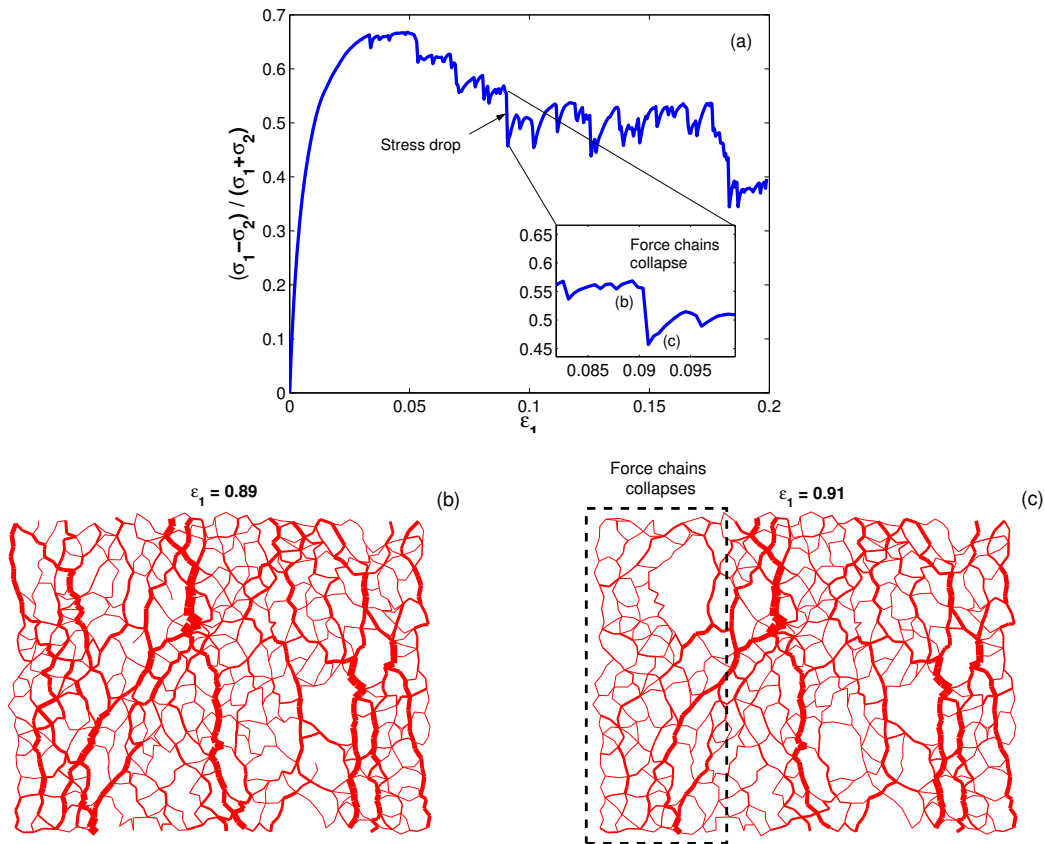


Figure 9. Stress drops (a) and their correlation with collapse of force chains: force network just before the stress drop (b) and right after it (c). The width of the lines is proportional to the magnitude of the contact force.

The coordination number  $Z$  is defined as the average of the number of contacts per particle. The evolution of the coordination number of one of the samples is presented in Figure 8. At low axial strain values, the dense system contracts and as a consequence a small increment of  $Z$  is observed. This is followed by a decrease of the  $Z$  value when the system dilates. This decrease is associated to the formation of force chains along the direction of loading and the breaking of interlocking between particles. As a result, each particle begins to lose contacts. This is macro-mechanically observed by the trend of dense samples to increase their volume. In contrast, the loose granular sample tends to a denser structure, and therefore new contacts are generated. Both samples around 8% axial strain reach a coordination number  $Z$  close to 3.3. This is close to the isostatic limit of  $Z = 3$  for two-dimensional granular assemblies, where internal rearrangements on slight variations of load are expected [29]. The isostatic limit is reached by means of the emergence of force chains, along which the low coordination number make them susceptible to collapse [8]. The collapse of force chains is reflected on an abrupt

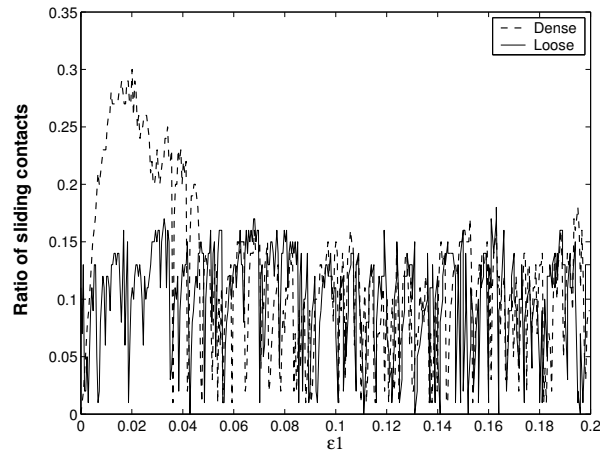


Figure 10. Evolution of the fraction of sliding contacts ratio during the biaxial test.

drop of stress. Between two collapses the force chains build up leading to an increase of the macroscopic friction coefficient.

In Figure 9 the direct relation between stress drops and collapse of force chains is presented. We selected one of the several stress drops as depicted in Figure 9(a). Then we plot the contact forces of the particles just before the stress drop Fig. 9(b) and right after it Fig. 9(c). Comparing these two force networks, one can see that some of the principal force chains after the stress drop have collapsed and therefore disappeared. This collapse drives the system to an internal rearrangement, in which particles undergo big relative displacements. The last is confirmed by the study of the displacement field of the individual particles [23], where big displacements of the particles are associated to abrupt reductions of the stress.

The microstructure of these collapses can be also visualized in the population of the sliding contacts. Figure 10 shows the evolution of the ratio between the number of sliding contacts and the total number of contacts. The sliding condition is given by the Coulomb's condition,  $F_t^c = \mu \cdot F_n^c$ . Initially, the dense medium has more sliding contacts when it contracts. Later when the sample begins to expand the number decreases. In general, the evolution of the sliding contacts for both systems during loading, consists of stages where their number increases, and short time "failures" where the fraction of sliding contacts jumps down.

Figure 11 compares the stress-strain evolution to the fraction of sliding contacts for the dense and loose sample. We observe more initial stability, with low frequency of jumps in the stress, in the dense sample. This stability is related to the average coordination number of the medium (Fig. 8), and the bigger this value the bigger the resulting stability of the granular skeleton. Although the jumps observed in the stress-strain behavior are less frequent than ones in the sliding contacts (Fig. 11), each stress jump is associated to an abrupt reduction of the number of sliding contacts. Each stress drop matches with a collapse of the fraction of sliding contacts.

These jumps in the deviator stress are present in realistic experiments of granular soils, but on a smaller scale [5, 6]. In our simulations the magnitude of these fluctuations can be partially attributed to the small size of the sample. One may ask the question if these

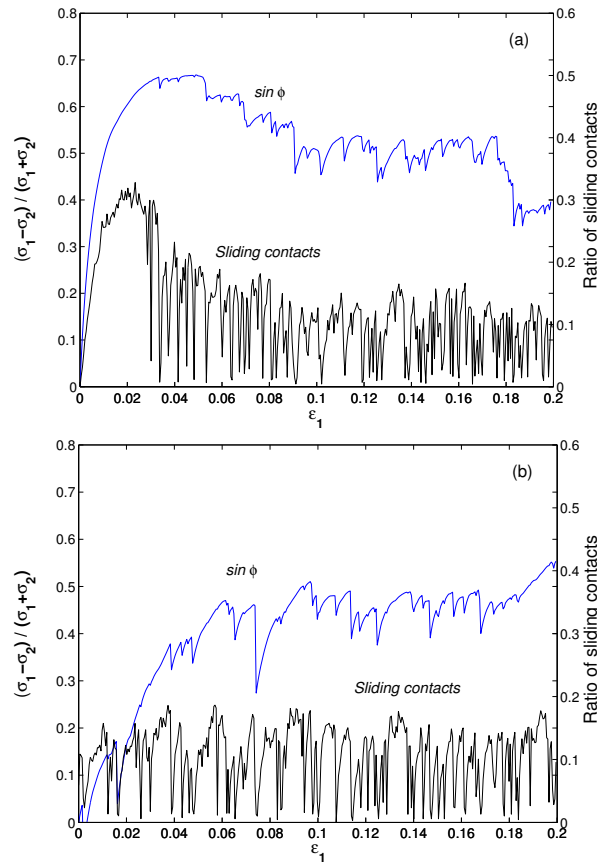


Figure 11. Evolution of stress-strain and the fraction of sliding contacts with axial strain (a) dense, (b) loose

fluctuations disappear as the size of the sample increases. Previous numerical simulations with the same model show that these fluctuations barely decrease as the number of particles of the specimen increases [30]. The distribution of energy released of these fluctuations in shear cell experiments follows approximately a power law [2]. The analogy of this statistic with the Gutenberg-Richter law suggests us that a detailed investigation of the collapse of force chains will improve our understanding of earthquakes.

## 5. DISCUSSION AND FINAL REMARKS

In this paper the effect of the initial density of the sample and the interparticle coefficient of friction on the macro-mechanical behavior of granular materials was investigated. The results show that at large strains the samples reach the critical state independent on their initial density, and they deform at constant void ratio, volume and mechanical coordination number. We have proven that for a wide range of contact friction coefficients, axial loading leads to

the same critical state. In this state the system approaches and retreats an unstable behavior leading to strong fluctuations of stress.

The stress drops were correlated to the evolution of the coordination number and the fraction of sliding contacts. We found that the granular sample at critical state develop force chains where the isostatic limit is reached. In this limit the force chains are highly susceptible to collapse, driven to strong stress fluctuations. Stress collapses remove the contacts from the sliding conditions, and therefore lead to a temporal stability in the granular sample. It is notable that the sliding contacts contribute substantially to determine the overall behavior at the critical state. This is different from the simulations [8] and experiment [31] on circular particles, where sliding plays a less important role. Future work will be oriented toward the study of the evolution of such force chains and the investigation of the nature of the stick-slip fluctuations at the critical state.

#### ACKNOWLEDGEMENTS

The authors want to acknowledge the support of the *Deutsche Forschungsgemeinschaft* Project HE 2732781 *Micromechanische Untersuchung des granulares Ratchetings*, and the EU project Degradation and Instabilities in Geomaterials with Application to Hazard Mitigation (DIGA) in the framework of the Human Potential Program, Research Training Networks (HPRN-CT-2002-00220). Alonso-Marroquin acknowledges the support of the Australian Research Council and the Australian Computational Earth System Simulator. Hans Herrmann acknowledges the Max-Planck Prize.

#### REFERENCES

1. Cundall PA, Strack ODL. A discrete numerical model for granular assemblies. *Géotechnique* 1979, 29(1): 47–65.
2. Tillemans HJ, Herrmann HJ. Simulating deformations of granular solids under shear. *Physica A* 1995, 217:261–288.
3. Mirghasemi A, Rothenburg L, Matyas E. Influence of particle shape on engineering properties of assemblies of two-dimensional polygon-shaped particles. *Geotechnique* 2002, 52:209–217.
4. Alonso-Marroquin F, Luding S, Herrmann HJ, Vardoulakis I. Role of the anisotropy in the elastoplastic response of a polygonal packing. *Phys. Rev. E* 2005, 51:051304.
5. Nasuno S, Kudrolli A, Bank A, Gollub JP. Time-resolved studies of stick-slip friction in sheared granular layers. *Phys. Rev. E* 1998, 58(2):2161–2171.
6. Adjemian F, Evesque P, Jia X. Ultrasonic experiment coupled with triaxial test for micro-seismicity detection in granular media. In R. García-Rojo, H.J. Herrmann, and S. McNamara, editors, *Powders and Grains 2005*, pages 281–285. Balkema, 2005.
7. Vardoulakis I, Georgopoulos IO. The stress - dilatancy hypothesis revisited: shear - banding related instabilities. *Soils & Foundations* 2005, 45:61–76.
8. Alonso-Marroquin F, Vardoulakis I, Herrmann HJ, Weatherley D, Mora P. Effect of rolling on dissipation in fault gouges. *Phys. Rev. E* 2006, 74:031306.
9. Lauritsen KB, Moukarzel C, Herrmann HJ. Statistical laws and mechanics of voronoi random lattices. *J. of Physique I* 1993, 3:1941–1951.
10. Kun F, Herrmann HJ. Fragmentation of colliding discs. *Int. J. of Mod. Phys. C* 1996, 7(6):837–855.
11. Kun F, Herrmann HJ. Transition from damage to fragmentation in collision of solids. *Phys. Rev. E*, 59 (3):2623–2632, 1999.
12. Alonso-Marroquin F, Herrmann HJ. Calculation of the incremental stress-strain relation of a polygonal packing. *Phys. Rev. E* 2002, 66:021301.
13. Bardet JP. *Experimental Soil Mechanics*. Prentice Hall, New Jersey, 1997.
14. Allen MP, Tildesley DJ. *Computer Simulation of Liquids*. Oxford University Press, Oxford, 1987.
15. Schofield AN, Wroth CP. *Critical State Soil Mechanics*. McGraw Hill, 1968.
16. Wood DM. *Soil behaviour and critical state soil mechanics*. ISBN: 0-521-33782-8, Cambridge, 1990.

17. Vardoulakis I. Shear band inclination and shear modulus of sand in biaxial tests. *Int. J. Numer. Anal. Meth. Geomech.* 1980, 4:103–119.
18. Desrues J. *Localization de la deformation plastique dans les materieux granulaires*. University of Grenoble, France, 1984.
19. Cundall PA. Numerical experiments on localization in frictional materials. *Ingenieur-Archiv* 1989, 59: 148–159.
20. Bardet JP, Proubet J. A numerical investigation of the structure of persistent shear bands in granular media. *Geotechnique* 1991, 41(4):599–613.
21. Vardoulakis I. Shear-banding and liquefaction in granular materials on the basis of a Cosserat continuum theory. *Ingenieur-Archiv* 1989, 59:106–113.
22. Chambon R, Caillerie R, Matsushima T. Plastic continuum with microstructure, local second gradient theories for geomaterials : localization studies. *International Journal of Solids and Structures* 2001, 38: 8503–8527.
23. Peña AA. *Simulación numérica de la respuesta esfuerzo deformación de medios granulares no cohesivos*. Universidad de los Andes, Bogotá D.C., Colombia., 2004.
24. Vermeer PA. The orientation of shear bands in biaxial tests. *Géotechnique* 1990, 40:223.
25. Roscoe FH. The influence of the strains in soil mechanics. *Geotechnique* 1970, 20(2):129–170.
26. Bardet JP Observations on the effects of particle rotations on the failure of idealized granular materials. *Mechanics of Materials* 1994, 18:159–182.
27. Skinner A. A note on the influence of interparticle friction on the shearing strength of a random assembly of spherical particles. *Geotechnique* 1969, 19(1):150–157.
28. Thornton C. Numerical simulations of deviatoric shear deformation of granular media. *Geotechnique* 2000, 50:43–53.
29. Moukarzel C. Isostatic phase transition and instability in stiff granular materials. *Phys. Rev. Lett.* 1998, 81:1634–1637.
30. García-Rojo R, McNamara S, Peña AA, Herrmann HJ. Sliding and localization in a biaxial test of granular material. In R. García-Rojo, H.J. Herrmann, and S. McNamara, editors, *Powders and Grains 2005*, pages 705–708. Balkema, 2005.
31. Oda M, Konishi J, Nemat-Nasser S. Experimental micromechanical evaluation of strength of granular materials: Effects of particle rolling. *Mechanics of Materials* 1982, 1:269–283.